TRENDS IN SCIENCES 2026; 23(10): 13491
https://doi.org/10.48048/tis.2026.13491 RESEARCH ARTICLE

Moisture Sorption Isotherms and Drying Kinetics of *Lepironia articulata*: Effects of Hot Air Drying on Mechanical Properties and Structural Changes

Pitchasak Chankuson[1,2], Sirikun Pethuan[3], Jureeporn Yuennan[1,2], Surasak Kaew-on[2] and Chaiporn Kaew-on[1,2,*]

[1]*Surface Technology Research Unit, Faculty of Science and Technology, Nakhon Si Thammarat Rajabhat University, Nakhon Si Thammarat 80280, Thailand*
[2]*Medical Instrumentation Physics Program, Faculty of Science and Technology, Nakhon Si Thammarat Rajabhat University, Nakhon Si Thammarat 80280, Thailand*
[3]*Biology Program, Faculty of Science and Technology, Nakhon Si Thammarat Rajabhat University, Nakhon Si Thammarat 80280, Thailand*

([*]Corresponding author's e-mail: chaiporn_kae@nstru.ac.th)

Received: 28 January 2026, Revised: 30 March 2026, Accepted: 10 April 2026, Published: 10 May 2026

Abstract

This study systematically investigates the moisture sorption behavior, drying kinetics, and coupled structural-mechanical responses of *Lepironia articulata* (LA) fiber under controlled hot-air drying conditions (40 - 80 °C). Equilibrium moisture content (EMC) was determined at water activity levels ranging from 0.1 to 0.9 and modeled using several empirical equations. Among these, the Modified Guggenheim-Anderson-de Boer (GAB) model provided the best fit across all temperatures, exhibiting the highest coefficient of determination (R^2) and lowest root mean square error (RMSE), indicating its suitability for describing sorption behavior in lignocellulosic fibers. Drying kinetics were analyzed using nine thin-layer drying models, where the Modified Page model consistently demonstrated superior predictive accuracy. The drying process was dominated by the falling-rate period, confirming that internal moisture diffusion governs mass transfer. Increasing drying temperature significantly accelerated moisture removal, reducing the drying time required to reach a moisture ratio of 0.10 from approximately 540 min at 40 °C to 140 min at 80 °C. Mechanical testing revealed a non-linear dependence of tensile strength on temperature, with an initial reduction at 40 - 50 °C, followed by recovery at 60 - 70 °C, and a maximum value at 80 °C, while elongation at break remained relatively stable. FTIR analysis indicated progressive dehydration, reduction of hydroxyl groups, and degradation of hemicellulose, accompanied by increased cellulose ordering. SEM observations confirmed corresponding morphological changes, including fiber densification at moderate temperatures and micro-crack formation and cell wall collapse at higher temperatures. The apparent contradiction between increased tensile strength and structural damage at elevated temperatures is explained by crystallinity-driven stiffening and improved microfibril alignment, which dominate bulk mechanical behavior despite localized defects. Overall, drying at 60 °C was identified as the optimal condition, providing a balance between efficient moisture removal, mechanical performance, and structural integrity. These findings provide a comprehensive framework for optimizing drying processes and enhancing the utilization of natural lignocellulosic fibers in sustainable material applications.

Keywords: Equilibrium moisture content, *Lepironia articulate*, Hot-air drying, Mathematic drying modeling

Introduction

Lepironia articulate (LA) is a herbaceous plant that grows in the Khuan Kreng swamp, a large swamp area located in the districts of Chian Yai, Cha-uat, Chaloem Phra Kiat, Huasai, and Ron Phibun of Nakhon Si Thammarat Province. Therefore, the population in

this area is engaged in weaving sedge products. However, one of the critical issues in the storage and utilization of the LA fibers is the growth of fungi under humid conditions. The high moisture content of the raw LA fibers provides a favorable environment for microbial contamination, leading to discoloration, odor formation, and deterioration of mechanical strength [1]. Therefore, an appropriate drying process is essential not only to reduce the moisture content but also to inhibit fungal growth without damaging the physical integrity of the fibers. Establishing the optimal drying conditions based on moisture desorption behavior can effectively minimize fungal contamination while maintaining the desirable physical and structural properties of the LA fibers. The mechanical strength and appearance of the LA fibers are highly influenced by their moisture content and drying conditions. An accurate understanding of moisture desorption isotherms is essential to optimize drying systems and prevent quality degradation [2]. Moisture sorption isotherms and drying kinetics are fundamental tools for understanding heat and mass transfer during the drying of plant-based materials and natural fibers. They describe both equilibrium moisture behavior and the rate of moisture removal under given thermal conditions [3].

Moisture sorption isotherms describe the relationship between equilibrium moisture content (EMC) and water activity (a_w) at constant temperature. They provide crucial data for modeling drying kinetics and designing industrial dryers. Several models, such as BET, Halsey, and GAB, have been used to predict sorption behavior; however, the modified GAB model provides better accuracy across a wide range of water activities and temperatures. The principle for determining the equilibrium humidity of the LA fibers involves exposing them to still air in a sealed container that maintains constant relative humidity and air temperature, until the humidity remains unchanged over time. A saturated salt solution controls the relative humidity of the air within the desired range, and a closed oven controls the air temperature [4]. To describe the relationship between equilibrium moisture content and water activity, several empirical and semi-theoretical models have been developed to fit moisture desorption isotherms of agricultural and lignocellulosic materials. Among these, the Modified Halsey, Modified Oswin, Modified Chung and Pfost, Modified Henderson, and Modified Guggenheim-Anderson-de Boer (GAB) models are most widely applied due to their flexibility and thermodynamic consistency. Each model provides distinct mathematical representations that capture sorption behavior under different temperature and humidity conditions. For example, the Modified Henderson model has been effectively used for cereal grains and bamboo fibers, while the Modified Oswin and Halsey models have been applied to describe desorption characteristics of rice husk and sugarcane bagasse [5]. The Modified GAB model, in particular, is considered the most reliable over a wide range of water activity (0.1 - 0.9) and temperature and has been successfully used for natural fibers such as kenaf, coir, and jute [6,7].

Drying kinetics and thin-layer drying models play a crucial role in understanding and optimizing moisture removal processes in lignocellulosic plant materials, particularly for wetland plants and natural fibers within the Cyperaceae family [8]. Drying kinetics describes the rate of moisture transport and evaporation during thermal treatment, while empirical and semi-theoretical drying models—such as Newton, Page, Modified Page, and Henderson and Pabis models—are widely applied to predict moisture ratio evolution and quantify the influence of drying temperature on mass transfer behavior [9]. These models provide essential parameters for evaluating drying efficiency, energy consumption, and process control, enabling the identification of optimal drying conditions that balance drying time with material quality preservation. For plants structurally similar to the LA fibers, inappropriate drying temperatures have been reported to induce excessive shrinkage, fiber collapse, and microstructural damage, resulting in deterioration of mechanical performance and long-term material stability [10,11].

Drying is an essential unit process in the treatment of plant-based materials because it significantly impacts moisture-related behavior, mechanical quality, and structure of the final product. Hot air drying is widely utilized because of its simplicity and cost-effectiveness; however, the drying temperature significantly influences the physical and chemical changes in plant tissues. High drying temperatures can accelerate moisture removal but may also cause negative changes in microstructure and material strength, which can affect product performance and use. The structural strength of

plant cell walls and fiber components is directly related to their mechanical properties, such as tensile strength, elongation at break, and stiffness. Moisture loss during drying modifies intermolecular interactions within the cell wall matrix, especially among cellulose, hemicellulose, and lignin, resulting in alterations in the stiffness and brittleness of plant materials. Several studies on natural fibers and agricultural products have demonstrated that increasing drying temperature can reduce mechanical strength due to structural collapse, microcracking, or fiber shrinkage [12,13]. The impacts are particularly significant in lignocellulosic plants, where temperature exposure destroys hydrogen bonding networks and damages load-bearing structures [14].

Spectroscopic and microscopic methods, including Fourier Transform Infrared Spectroscopy (FTIR) and Scanning Electron Microscopy (SEM), are often used for understanding these structural changes. FTIR analysis enables the identification of chemical functional groups and provides insights into modifications of molecular bonds caused by thermal treatment. Variations in characteristic absorption bands associated with hydroxyl, carbonyl, and polysaccharide groups have been reported following hot air drying, indicating changes in chemical composition or bonding environments within plant fibers [15]. Meanwhile, SEM offers direct visualization of surface morphology and internal microstructure, revealing phenomena such as cell wall deformation, pore collapse, and fracture formation that are often correlated with mechanical degradation at elevated temperatures [16,17]. Previous studies into plant materials, such as bamboo, jute, apple tissues, and other fibrous crops, have shown a significant correlation among drying temperature, microstructural development, and mechanical properties. For instance, higher drying temperatures have been shown to cause significant shrinkage and microcrack formation in plant fibers, resulting in reduced tensile strength and flexibility [18]. These results show the need of controlling drying conditions to maintain both structural integrity and the functional properties of plant materials.

Despite extensive studies on drying behavior of various lignocellulosic materials, there is a lack of systematic investigation on *Lepironia articulata* fibers, particularly in terms of moisture desorption behavior, drying kinetics, and coupled structural–mechanical responses under controlled drying conditions. Furthermore, most existing studies treat moisture behavior, structural evolution, and mechanical properties separately, resulting in a limited understanding of their interdependence.

Therefore, the novelty of this study lies in the integrated investigation of moisture sorption isotherms, drying kinetics, and multi-scale structural and mechanical changes of LA fibers under hot-air drying conditions. This work combines modeling, experimental validation, and advanced characterization techniques (SEM, FTIR, and tensile testing) to provide a comprehensive understanding of drying-induced transformations. The findings offer both scientific and practical significance by enabling optimized drying strategies, improving product quality, and supporting sustainable utilization of natural fibers.

Materials and methods

Sample preparation

The LA fibers used in the experiment were from Cha-uat District, Nakhon Si Thammarat Province. It had been woven but had yet to undergo any decoration steps. Samples were cut into 5×5 cm² pieces with an average thickness of 1.6 ± 0.1 mm, as shown in **Figure 1**. All samples were kept in sealed polyethylene bags before testing to avoid moisture variation.

Figure 1 The LA fiber sample for the experiment.

Analyzing the moisture sorption isotherms of the LA fiber

The equilibrium moisture content of the LA sample was determined by placing 5 saturated salt solutions, namely LiCl, $MgCl_2 \cdot 6H_2O$, $Mg(NO_3)_2 \cdot 6H_2O$, NaCl, and KNO_3, into 3 sets of glass bottles each. In this experiment, 5 saturated salt solutions were employed to establish equilibrium moisture content. The resulting ambient temperatures (40 - 60 °C) and water activity levels (0.1 - 0.9, decimal) are presented in **Table 1**. Then, weigh the LA sample using a high-precision digital analytical balance with a resolution of 0.0001 g (Sartorius, Germany). Put the LA sample into the stainless-steel strainer inside the glass bottle, then close the lid tightly and place it in the oven at 40, 50, 60, 70, and 80 °C to allow the LA sample's humidity to reach balance. When the LA sample's weight remained unchanged after 3 consecutive weight measurements, the moisture content was determined following the AOAC method [19]. The final moisture content of the LA sample implies the EMC value, which occurred among static surrounding conditions. Schematic representation of the experimental methodology for determining the EMC of LA fiber at temperatures ranging from 40 to 80 °C, according to **Figure 2**.

Table 1 The water activity values (expressed in decimal form) corresponding to the saturated salt solutions at temperatures of 40, 50, 60, 70, and 80 °C.

Salt solutions	Temperature (°C)				
	40	50	60	70	80
LiCl	0.1121	0.1110	0.1095	0.1075	0.1051
$MgCl_2 \cdot 6H_2O$	0.3160	0.3054	0.2926	0.2777	0.2605
$Mg(NO_3)_2 \cdot 6H_2O$	0.5060	0.4890	0.4730	0.4580	0.4415
NaCl	0.7468	0.7443	0.7450	0.7506	0.7629
KNO_3	0.8903	0.8478	0.8110	0.7704	0.7308

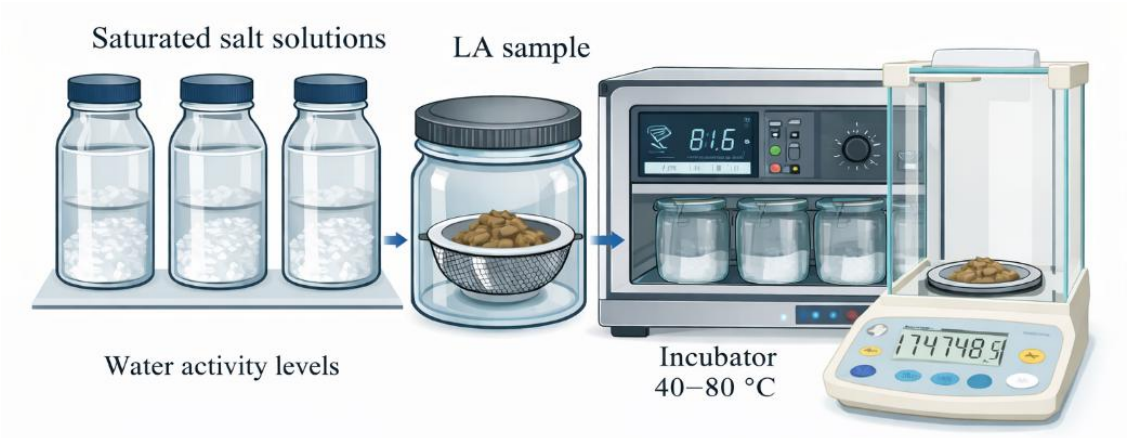

Figure 2 The experimental setup used for moisture sorption isotherm analysis of LA fiber at different temperatures.

Mathematical models of sorption isotherms

The LA sample weight was evaluated by triplication. **Table 2** shows the conventional sorption isotherm models chosen to predict the EMC values that fit the experimental data in Eqs. (1) - (5).

Table 2 Mathematical model for prediction the equilibrium moisture content.

Name of model	EMC equation model	
Modified Halsey [20]	$EMC = \left[\frac{-\ln a_w}{\exp(A+B\cdot T)}\right]^{-(1/C)}$	(1)
Modified Oswin [21]	$EMC = (A + B \cdot T) \cdot \left[\frac{a_w}{(1-a_w)}\right]^{1/C}$	(2)
Modified Chung & Pfost [22]	$EMC = \frac{-1}{C}\ln\left[-\frac{(T+B)}{A}\ln a_w\right]$	(3)
Modified Henderson [23]	$EMC = \left[\frac{\ln(1-a_w)}{(-A\cdot(T+B))}\right]^{1/C}$	(4)
Modified GAB [24-26]	$EMC = \frac{A\cdot B\cdot\left(\frac{C}{T}\right)\cdot a_w}{(1-B\cdot a_w)\left[1-B\cdot a_w+\left(\frac{C}{T}\right)\cdot B\cdot a_w\right]}$	(5)

Note: a_w is the water activity (decimal), *EMC* is the equilibrium moisture content (%dry basis), *T* is the temperature (K) and *A*, *B* and *C* are arbitrary coefficients of models.

The statistical principle for selecting the most suitable equation to describe the EMC process is the highest coefficient of determination value (R^2), and the lowest root mean square error (RMSE) value. The 2 statistic parameters can be calculated by Eqs. (6) and (7), respectively:

$$R^2 = \frac{\sum(M_e - M_p)^2}{\sum M_e^2 \sum M_p^2} \quad (6)$$

$$RMRE = \sqrt{\frac{1}{N}\sum(M_e - M_p)^2} \quad (7)$$

where M_p is the predicted value of data, M_e is the experimental value of data, is the mean of the experimental values, and N is the number of experimental points.

To verify model robustness and avoid possible ove r-fitting of the equation, a sensitivity analysis was perfor med by altering each parameter (± 5%) and recalculatin g RMSE. Negligible RMSE change (< 1%) confirmed model stability.

Determination of drying kinetics and drying models

The initial moisture content (IMC) of the LA fiber was evaluated using the AOAC standard method. The fresh LA fibers in this experiment had an IMC of 78 ± 2% (wet basis). Maintaining similar IMC ensures that observed differences in drying rate are attributable solel y to temperature effects rather than starting moisture un evenness. Drying studies were conducted with a laboratory-scale hot air oven with forced air circulation. The drying air temperatures were established at 40, 50, 60, 70, and 80 °C, respectively. The air velocity was kept at 1.0 ± 0.1 ms^{-1}, and ambient relative humidity was 50 ± 3%. Equal sample masses were used for replicates (n = 3). Before adding the samples, the oven was operated until the temperature settled. Each drying iteration was done using approximately equivalent initial sample weights, and all experimental procedures were executed in triplicate.

$$MR = \frac{M_t - M_e}{M_0 - M_e} \quad (8)$$

where M_t is the moisture content at time t, M_0 is the initial moisture content, and M_e is the equilibrium moisture content.

LA's drying behavior was described by fitting experimental MR-time data to thin-layer drying models, whose mathematical formulas are in **Table 3**. Model parameters were estimated using least-squares fitting in nonlinear regression analysis. R^2 and RMSE were used to determine fit quality by Eqs. (9) to (17).

Table 3 Mathematical models for drying to predict the behavior of drying kinetics.

Drying kinetic model	Equation	
Newton [27,28]	$MR = \exp(-kt)$	(9)
Page [29-31]	$MR = \exp(-kt^n)$	(10)
Modified Page [29-31]	$MR = \exp(-kt)^n$	(11)
Logistic [30]	$MR = \frac{a}{(1+\exp(kt))}$	(12)
Henderson and Pabis [30,32,33]	$MR = a\exp(-kt)$	(13)
Logarithmic [28,30]	$MR = a\exp(-kt)$+c	(14)
Two-term exponential [30,32,34]	$MR = a\exp(-kt) + (1-a)\exp(-kat)$	(15)
Approximation of diffusion [28,30]	$MR = a\exp(-kt) + (1-a)\exp(-kbt)$	(16)
Verma *et al.* [30]	$MR = a\exp(-kt) + (1-a)\exp(-kgt)$	(17)

Note: a, k and n are arbitrary constants of drying kinetic model, t is drying time (min).

The optimal drying time for each drying temperature was defined based on a combined kinetic and practical criterion. Specifically, the drying time corresponding to a moisture ratio of MR = 0.10 was selected as the target endpoint, as this level is widely accepted as sufficient for dimensional stability and safe storage of natural fiber materials.

The drying time required to reach MR = 0.10 was determined from the best-fitting drying model for each temperature. In addition, the total drying time required to achieve a constant mass condition was recorded for comparison.

Examination of mechanical properties and structural alterations

The optimal drying time determined from previous experiments was used as the drying time for the LA fiber at different temperatures to study the effect of hot air temperature on the mechanical properties and structural changes of the LA fiber.

Mechanical properties

Tensile testing has been done on the LA fiber to evaluate their mechanical properties. A tensile testing machine (Zwick Roell, Germany) with a 1.0 kN load cell and a test speed of 50 mm/min was used to test each sample 5 times. Tensile strength (σ) was calculated as the maximum load sustained by the specimen divided by the initial cross-sectional area. Elongation at break (ε) was determined from the ratio of the extension at fracture to the original gauge length and expressed as a percentage. At least 5 specimens were tested per drying condition (n ≥ 5). Results are reported as mean ± standard deviation. One-way ANOVA followed by Tukey's HSD post-hoc test ($p < 0.05$) was applied to assess the statistical significance of differences in tensile strength and elongation at break among drying temperatures.

FTIR analysis

The surface chemical bonding of the LA fiber was analyzed using Attenuated Total Reflection-Fourier Transform Infrared Spectroscopy (ATR-FTIR). This investigation aimed at understanding the molecular interactions occurring on the fiber surface. Infrared spectra were obtained using an INVENIOS Bruker spectrometer (Germany) fitted with a diamond ATR crystal, over the wavenumber range of 4,000 - 500 cm^{-1}.

Scanning Electron Microscopy (SEM)

The microstructural characteristics of the dried LA fiber were examined using Scanning Electron Microscopy (Hitachi, Japan). Samples were mounted on aluminum stubs using double-sided adhesive tape and sputter-coated with gold-palladium. The observations were conducted at an accelerating voltage of 5 kV with magnifications of 250×, 2,000×, and 5,000×.

Results and discussion

The equilibrium moisture content (EMC)

From the experimental set up, the experimental data of the EMC value of the LA fibers varieties were determined by following the standard AOAC method for a surrounding temperature ranging of 40, 50, 60, 70

and 80 °C which correlated to the water activity ranging of 0.1 - 0.9 (decimal). These experimental values were statistically analyzed by non-linear regression methods. The best fitted coefficients of the EMC equations were simulated and shown in **Table 4**.

The results showed that the simulated results using the Modified GAB model have a strong relationship to the experimental results of both the LA fibers varieties (the highest R^2 value and the lowest RMSE). From the experimental results, the conclusion of the study of the EMC value of the LA fibers states that at the constant temperature the EMC value depends on the relative humidity of air surrounding. When the surrounding relative humidity decreases, the EMC value of the LA fibers varieties decreases, respectively. This is because the water vapor transfer between surrounding air and the LA fiber is high at the low surrounding relative humidity [5]. On the other hand, with constant relative humidity, the EMC value is relatively dependent on the surrounding temperature. This is because the heat reduces the binding force in the water molecules. All of the mechanisms for transferring water vapor between the LA fibers and the surrounding air correspond to the other previous works that reported on EMC values of different samples [6,7].

Table 4 Arbitrary constant of EMC model for the LA fiber in water activity ranging of 0.1 - 0.9 (decimal).

Temperature	Model	Parameter			R^2	RMSE
		A	B	C		
40 °C	Modified Halsey	−225.2819	0.7323	1.5639	0.9770	2.0818
	Modified Oswin	134.3464	−0.3767	1.9646	0.9939	1.0746
	Modified Chung-Pfost	271.6316	−209.1357	0.0715	0.9884	1.4764
	Modified Handerson	3.7858×10^{-5}	1.0010	1.1223	0.9978	0.4157
	Modified GAB	13.8479	0.8112	1193.5225	**0.9994**	**0.3325**
50 °C	Modified Halsey	2.3119	0.0037	1.5052	0.9831	1.5095
	Modified Oswin	14.4875	−0.0026	1.8997	0.9966	0.6794
	Modified Chung-Pfost	264.8016	−220.6734	0.0843	0.9841	1.4617
	Modified Handerson	9.7600×10^{-5}	1.1078	1.1631	0.9984	0.4564
	Modified GAB	10.6373	0.8396	1391.6652	**0.9997**	**0.2140**
60 °C	Modified Halsey	4.0473	−0.0027	1.4749	0.9802	1.3841
	Modified Oswin	3.0757	0.0253	1.8712	0.9954	0.6683
	Modified Chung-Pfost	293.8841	−217.5559	0.0983	0.9869	1.1261
	Modified Handerson	0.0001	1.2233	1.1557	0.9986	0.3672
	Modified GAB	9.3646	0.8326	1295.5073	**0.9997**	**0.1843**
70 °C	Modified Halsey	1.6431	0.0031	1.4109	0.9846	1.0606
	Modified Oswin	12.0099	−0.0076	1.7872	0.9963	0.5231
	Modified Chung-Pfost	239.0028	−246.1592	0.1145	0.9783	1.2574
	Modified Handerson	0.0002	0.8873	1.0989	0.9953	0.5858
	Modified GAB	6.9801	0.8703	1,506.1543	**0.9993**	**0.3471**
80 °C	Modified	2.3725	−0.0003	1.4107	0.9814	0.9125
	Halsey	12.7839	−0.0155	1.7946	0.9960	0.4210
	Modified	266.1174	−245.0084	0.1472	0.9858	0.7960
	Oswin	0.0002	0.9404	1.1107	0.9987	0.2346
	Modified	2.3725	−0.0003	1.4107	0.9814	0.9125

Figure 3 illustrates the experimental and predicted moisture sorption isotherms of the LA fibers at temperatures of 40, 50, 60, 70, and 80 °C. The sorption characteristics of the LA fibers exhibit the classical temperature-dependent behavior typical of lignocellulosic materials. The EMC decreases with increasing temperature due to the weakening of hydrogen bonds between water molecules and hydroxyl

groups in lignin, hemicellulose, and cellulose. Increases in heat energy cause a reduction in the binding affinity of water and fiber components. This finding aligns with previous research on kenaf, jute, and flax fibers, among others, which showed reduced hygroscopicity when subjected to elevated temperatures [35,36]. At higher a_w values, the EMC increases exponentially, indicating multilayer moisture adsorption and capillary condensation. This behavior is consistent with the GAB isotherm commonly found in natural fibers and wetland plants. The structure of the LA fibers, which has high porosity and a well-developed capillary network, favors this activity, which is similar to what has been observed in wetland rush fibers [37].

The EMC of the LA fiber was examined at various temperatures and water activities, using a modified GAB model to suit experimental isotherms. The predicted curves closely match the actual data at all temperatures, which shows that the model is good at predicting how lignocellulosic plant fibers absorb water. Minimal differences between the observed and computed EMC values show that the model is good for both practical use and scientific study [38]. It is important to note that the difference between the prediction curves is bigger for high water activity levels ($a_w > 0.6$), especially at 60 °C. This gap becoming bigger illustrates that EMC's sensitivity to temperature goes up when there is a lot of moisture. This is because molecules may move around more easily, and the energy needed to bond fibers and water goes down at higher temperatures. These results are consistent with known facts about various plant leaves and fibers, where isotherm forms and their temperature variations are essential for enhancing industrial drying and storage [39].

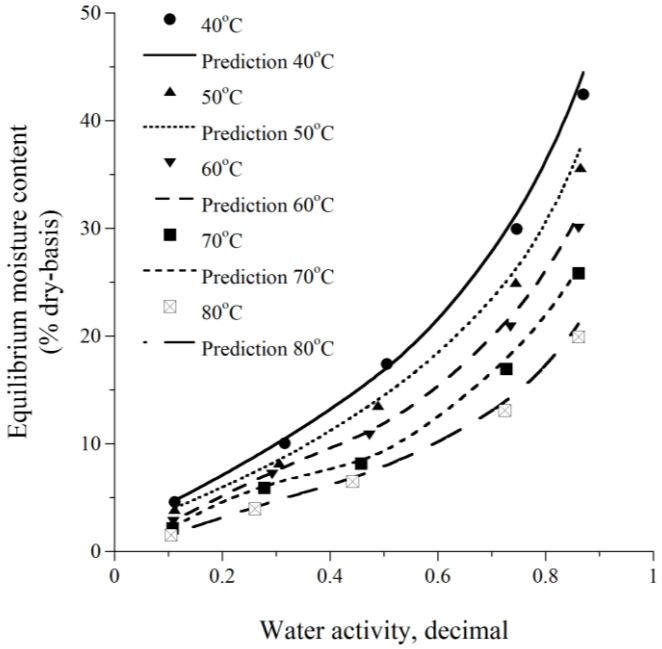

Figure 3 Comparison of the experimental data (dot) and predicted data (line) of the equilibrium moisture content models of the LA fibers variety among surrounding water activity and surrounding temperature of 0.1 - 0.9 (decimal) and of 40 - 80 °C, respectively.

A comprehensive understanding of desorption behavior is crucial for optimizing hot-air drying conditions to achieve efficient moisture removal while preserving the mechanical strength and microstructural integrity of the fibers. Accurate modeling of the EMC minimizes risks of deterioration such as fungal contamination and deformation, enabling the design of temperature-specific drying strategies [40]. The modified GAB model demonstrated a strong predictive capability for the LA fiber and can potentially be applied to other hydrophytic plant materials with similar characteristics.

The drying kinetics and drying models

To determine the optimal hot-air drying time for LA fiber, drying kinetic models were employed to describe the relationship between moisture ratio (MR) and drying time (**Figure 4**). Thin-layer drying models are widely used to characterize moisture removal behavior and predict drying kinetics under controlled thermal conditions [41]. The selected models represent different moisture transport mechanisms in lignocellulosic materials. The Newton model describes simple exponential decay associated with external mass transfer, whereas semi-empirical models such as Page, Modified Page, and Logarithmic incorporate additional parameters to account for internal diffusion and structural heterogeneity. More complex models, including the 2-term exponential, approximation of diffusion, and Verma models, are capable of representing multi-stage drying behavior [42,43]. Model performance was evaluated by fitting MR-time data using the coefficient of determination (R^2) and root mean square error (RMSE), with fitted parameters summarized in **Table 5**.

Figure 4 shows that MR decreased continuously with drying time at all temperatures (40 - 80 °C), with higher temperatures significantly accelerating moisture removal. The drying process was dominated by the falling-rate period, indicating that internal diffusion governs moisture transport. The time required to reach MR ≈ 0.10 decreased from approximately 540 min at 40 °C to 140 min at 80 °C, confirming the strong influence of temperature on drying kinetics [41-44]. This acceleration is attributed to increased vapor pressure gradients and reduced water viscosity at elevated temperatures, consistent with observations in other agricultural materials such as turmeric and ginger [45,46]. However, excessively high temperatures (70 - 80 °C) may induce structural damage, including shrinkage and microcracking, which can affect material properties [47,48].

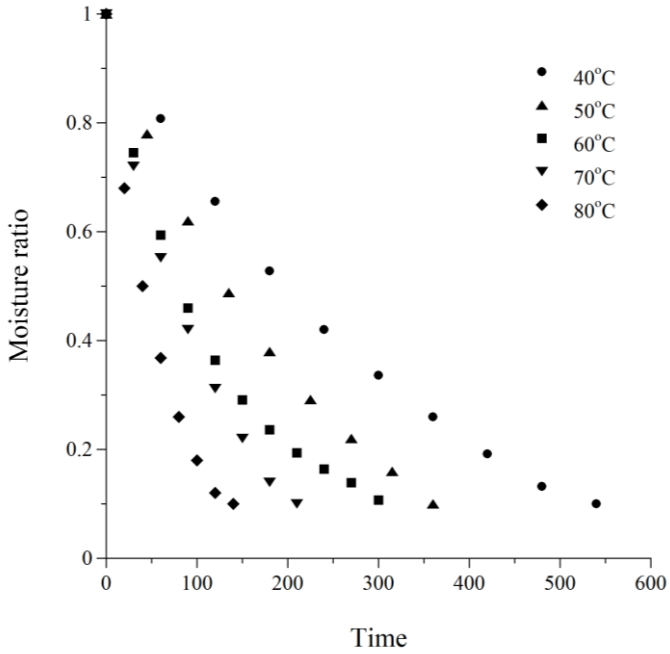

Figure 4 Comparison of the moisture ratio for the LA fiber drying at temperatures of 40, 50, 60, 70, and 80 °C.

The drying kinetics of LA fiber at different temperatures (40–80°C) were evaluated using nine thin-layer drying models, as presented in **Table 5**. Among all models, the Modified Page model consistently provided the best fit to the experimental data across all temperatures, exhibiting the highest coefficient of determination (R^2 = 0.994 - 0.996) and the lowest root mean square error (RMSE = 0.016 - 0.021). This superior performance can be attributed to its ability to account for both external mass transfer and internal moisture diffusion mechanisms, which are critical in

lignocellulosic materials with heterogeneous structures [49,50].

The drying rate constant (k) increased significantly with temperature, ranging from 0.0012 at 40 °C to 0.0094 at 80 °C, indicating enhanced moisture diffusivity at higher thermal conditions. This trend is consistent with the Arrhenius-type behavior of effective moisture diffusivity, where increased temperature reduces water viscosity and promotes vapor diffusion within the fiber matrix [51]. Similarly, the exponent (n) in the Modified Page model increased slightly with temperature, suggesting a greater contribution of internal diffusion resistance and structural changes during drying.

Notably, the lowest RMSE value was observed at 60 - 70 °C, indicating optimal model predictability and stable drying behavior within this temperature range. In contrast, at 80 °C, although the drying rate was highest, a slight increase in RMSE was observed, which may be associated with structural alterations such as fiber shrinkage, collapse, and micro-crack formation. These structural changes can disrupt moisture transport pathways, leading to deviations from ideal drying behavior [52].

Other models, such as Page, 2-term exponential, and Verma, also showed good agreement with experimental data ($R^2 > 0.99$), but their performance was consistently inferior to the Modified Page model. Simpler models like Newton, Henderson, and Pabis exhibited lower accuracy, particularly at extreme temperatures, due to their inability to capture complex moisture migration mechanisms.

Thus, the results confirm that the Modified Page model is the most suitable for describing the drying kinetics of LA fiber over a wide temperature range and can be effectively used for process optimization and dryer design. The improved performance of Page-type models is consistent with previous studies on plant biomaterials. For example, the Page model effectively described drying behavior in *Pereskia* leaf powders [45], while both Page and 2-term models accurately captured drying kinetics in turmeric across varying temperatures [53]. These findings highlight the importance of model selection in accurately representing moisture transport in heterogeneous biological matrices.

Table 5 Kinetic drying model parameters and statistical evaluation for LA fiber at different temperatures (40 - 80 °C).

Temperature	Drying kinetic model	Arbitrary constants	R^2	RMSE
40 °C	Newton	k = 0.0010	0.975	0.055
	Page	k = 0.0011, a = 1.15	0.991	0.026
	Modified Page	**k = 0.0012, n = 1.18**	**0.994**	**0.021**
	Logistic	k = 0.0013, a = 1.05	0.989	0.029
	Henderson and Pabis	k = 0.0011, a = 1.02	0.985	0.034
	Logarithmic	k = 0.0011, a = 1.00, b = −0.010	0.990	0.027
	Two-term exponential	k = 0.0013, a = 0.52	0.992	0.024
	Approximation of diffusion	k = 0.0012, a = 0.55, b = 0.0008	0.991	0.025
	Verma	k = 0.0012, a = 0.58, g = 0.0009	0.992	0.024
50 °C	Newton	k = 0.0020	0.978	0.048
	Page	k = 0.0022, a = 1.22	0.993	0.021
	Modified Page	**k = 0.0023, n = 1.25**	**0.996**	**0.018**
	Logistic	k = 0.0025, a = 1.08	0.991	0.024
	Henderson and Pabis	k = 0.0021, a = 1.04	0.987	0.029
	Logarithmic	k = 0.0022, a = 1.01, b = −0.012	0.992	0.022
	Two-term exponential	k = 0.0024, a = 0.55	0.994	0.020
	Approximation of diffusion	k = 0.0023, a = 0.58, b = 0.0009	0.993	0.021
	Verma	k = 0.0023, a = 0.60, g = 0.0010	0.994	0.020

Temperature	Drying kinetic model	Arbitrary constants	R^2	RMSE
60°C	Newton	k = 0.0032	0.981	0.043
	Page	k = 0.0036, a = 1.28	0.995	0.018
	Modified Page	**k = 0.0038, n = 1.32**	**0.997**	**0.014**
	Logistic	k = 0.0041, a = 1.12	0.992	0.022
	Henderson and Pabis	k = 0.0035, a = 1.06	0.989	0.028
	Logarithmic	k = 0.0036, a = 1.02, b = -0.015	0.994	0.019
	Two-term exponential	k = 0.0039, a = 0.58	0.996	0.016
	Approximation of diffusion	k = 0.0040, a = 0.61, b = 0.0011	0.995	0.018
	Verma	k = 0.0037, a = 0.64, g = 0.0013	0.996	0.017
70°C	Newton	k = 0.0055	0.980	0.046
	Page	k = 0.0058, a = 1.35	0.994	0.019
	Modified Page	**k = 0.0061, n = 1.38**	**0.996**	**0.016**
	Logistic	k = 0.0063, a = 1.15	0.992	0.022
	Henderson and Pabis	k = 0.0056, a = 1.08	0.988	0.027
	Logarithmic	k = 0.0058, a = 1.03, b = −0.017	0.993	0.020
	Two-term exponential	k = 0.0062, a = 0.60	0.995	0.018
	Approximation of diffusion	k = 0.0060, a = 0.63, b = 0.0012	0.994	0.019
	Verma	k = 0.0060, a = 0.66, g = 0.0014	0.995	0.018
80°C	Newton	k = 0.0085	0.978	0.050
	Page	k = 0.0090, a = 1.40	0.993	0.022
	Modified Page	**k = 0.0094, n = 1.42**	**0.995**	**0.019**
	Logistic	k = 0.0098, a = 1.18	0.991	0.025
	Henderson and Pabis	k = 0.0087, a = 1.10	0.987	0.030
	Logarithmic	k = 0.0090, a = 1.05, b = −0.020	0.992	0.023
	Two-term exponential	k = 0.0096, a = 0.63	0.994	0.021
	Approximation of diffusion	k = 0.0093, a = 0.66, b = 0.0015	0.993	0.022
	Verma	k = 0.0092, a = 0.69, g = 0.0016	0.994	0.021

Table 6 Modified Page model fitting parameters and statistical indicators for hot air drying of the LA fiber at different temperatures.

Temperature (°C)	k	n	R^2	RMSE
40	0.0012	1.18	0.994	0.021
50	0.0023	1.25	0.996	0.018
60	**0.0038**	**1.32**	**0.997**	**0.014**
70	0.0061	1.38	0.996	0.016
80	0.0094	1.42	0.995	0.019

The Modified Page model was further applied to describe drying behavior across the temperature range of 40 - 80 °C, with kinetic parameters (k and n) and statistical indicators presented in **Table 6**. The drying constant (k) increased with temperature, from 0.0012 at 40 °C to 0.0094 at 80 °C, indicating enhanced effective

moisture diffusivity. Similarly, the exponent (n) increased with temperature, reflecting stronger nonlinearity in moisture removal behavior and confirming the increasing dominance of internal diffusion mechanisms at higher temperatures [54]. These trends are consistent with previous studies on plant materials such as jackfruit slices and spinach leaves, where increased drying temperatures resulted in higher drying constants and improved model fitting [55,56].

The Modified Page model exhibited excellent agreement with experimental data across all temperatures ($R^2 \geq 0.994$), with the lowest RMSE observed at 60 °C (0.014). This suggests that moderate drying conditions provide an optimal balance between diffusion-driven moisture transport and structural stability. Slight increases in RMSE at higher temperatures (70 - 80 °C) may be attributed to structural changes such as shrinkage and microcracking, which introduce variability not fully captured by empirical models [57].

The improved model accuracy at moderate temperatures indicates that drying kinetics are more predictable under conditions where diffusion dominates without significant thermal damage. This observation is consistent with previous studies reporting superior performance of Page-type models in describing nonlinear drying behavior in biomaterials, including bird's eye chili [58,59]. From a practical perspective, increasing drying temperature enhances moisture diffusivity and reduces drying time; however, excessive temperatures may compromise product quality. Therefore, accurate kinetic modeling is essential for optimizing drying conditions and improving energy efficiency. Empirical models such as the Modified Page model are widely recognized for their robustness and applicability across a range of plant materials and drying conditions [60,61].

Overall, the consistent increase in k and n with temperature, together with high R^2 values, confirms that the Modified Page model provides a reliable framework for describing the drying kinetics of LA fiber. Its strong performance across all tested conditions supports its application for predicting drying time and guiding industrial drying process design. Furthermore, these results emphasize that model evaluation should consider performance across multiple temperatures to ensure generalizability, rather than relying on single-condition assessments [62].

Examine mechanical properties and structural alterations

The LA fiber was dried in a hot air oven with a controlled air temperature of 40, 50, 60, 70, and 80 °C for 5 h at each temperature. The mechanical characteristics and structural changes of the LA fiber was investigated in relation to the hot air temperature.

Mechanical properties

The stress-strain curves of the LA fibers under control and after hot air drying at 40, 50, 60, 70, and 80 °C are presented in **Figure 5**. The control samples exhibit the highest overall mechanical performance, characterized by greater ultimate stress and strain at break, indicating superior load-bearing capacity and flexibility. This behavior suggests that the native moisture content plays a crucial role in maintaining intermolecular bonding and structural integrity within the lignocellulosic fiber matrix. At 40 °C, the stress-strain response remains relatively comparable to the control samples, with only a slight reduction in tensile strength and elongation at break. This indicates that mild drying removes free and loosely bound water without causing significant disruption to the cell wall structure. However, as the drying temperature increases to 50 and 60 °C, a noticeable decrease in maximum stress and strain is observed. The fibers become stiffer and exhibit a more brittle failure behavior, reflecting reduced plastic deformation before fracture. At increased temperatures of 70 and 80 °C, the stress-strain curves show a significant reduction in tensile strength and elongation at break. Although some samples demonstrate higher initial stiffness (a steeper slope in the elastic region), premature failure occurs at reduced strain values. This indicates that excessive temperature exposure results in structural damage, limiting the fiber's propensity to distribute stress during deformation.

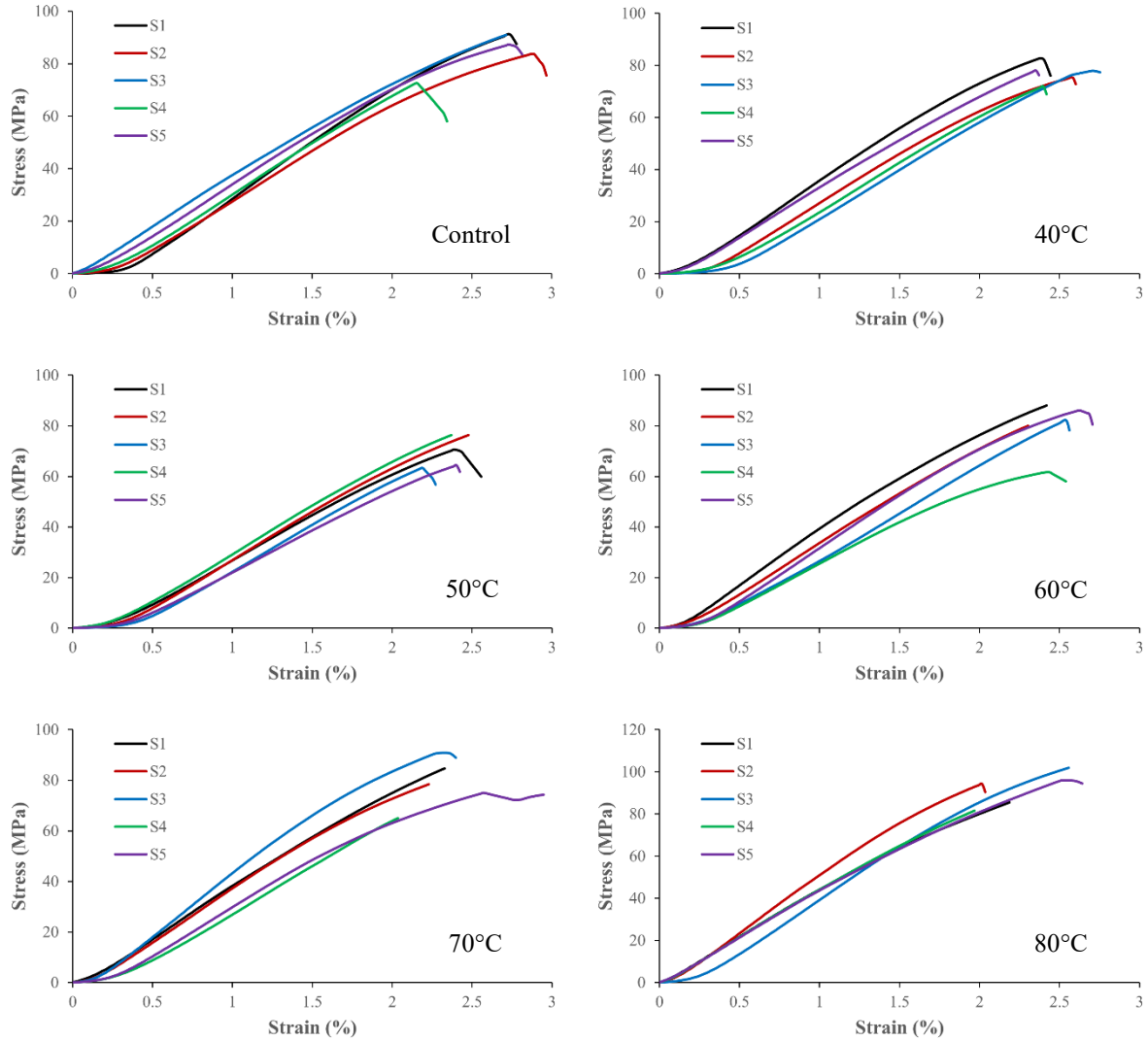

Figure 5 Stress-Strain curves of the LA fiber control and drying at temperatures of 40, 50, 60, 70, and 80 °C.

The reduction in mechanical properties of LA fibers at higher drying temperatures may be related to moisture-induced structural and chemical changes inside the lignocellulosic cell wall. Moisture functions as a natural plasticizer, enhancing molecular mobility and flexibility; therefore, its removal during drying initially increases stiffness but progressively reduces ductility [15]. At drying temperatures of 40 - 50 °C, moisture loss is mainly associated with free and loosely bound water, resulting in minimal reductions in tensile strength and elongation at break, which is consistent with observations in other natural plant fibers [63]. However, drying at higher temperatures promotes excessive removal of bound water, leading to microfibril shrinkage, cell wall collapse, and microcrack formation, thereby limiting stress redistribution and causing premature fracture, as reflected by the reduced strain at break in the stress-strain [18]. Similar temperature-dependent transitions from ductile to brittle behavior have been widely reported in lignocellulosic fibers and biocomposites subjected to thermal drying [64]. Recent reviews also support these findings, emphasizing that inappropriate drying conditions accelerate mechanical degradation despite improved drying efficiency [13].

Tensile strength and elongation at break of LA fibers at different temperatures are among the mechanical property testing results presented in **Table 7**.

Table 7 Mechanical properties results: tensile strength, and elongation at break of the LA fiber with different temperature.

LA samples	Tensile strength (MPa)	Elongation at break (%)
Control	85.14 ± 7.62^{ab}	2.64 ± 0.28^{ab}
40 °C	77.23 ± 3.97^{a}	2.48 ± 0.15^{a}
50 °C	71.24 ± 7.68^{a}	2.42 ± 0.18^{a}
60 °C	80.68 ± 11.81^{ab}	2.51 ± 0.15^{ab}
70 °C	79.74 ± 9.98^{ab}	2.34 ± 0.20^{ab}
80 °C	100.63 ± 5.75^{b}	2.57 ± 0.39^{b}

Note: Different superscript letters within the same column indicate significant differences ($p < 0.05$) according to Tukey's test.

The mechanical properties of LA fibers as a function of drying temperature are summarized in **Table 7**. Tensile strength exhibited a non-linear response to temperature, with a significant reduction at 40 - 50 °C (77.23 - 71.24 MPa; Tukey group "a") compared to the control (85.14 MPa; "ab"), followed by partial recovery at 60 - 70 °C (79.74 - 80.68 MPa; "ab"), and a pronounced increase at 80 °C (100.63 MPa; "b"). This statistical grouping confirms that only the highest drying temperature induced a distinct mechanical response, while intermediate temperatures remained statistically comparable to the untreated fiber.

The initial reduction in tensile strength at 40 - 50 °C can be attributed to early-stage thermal softening and partial degradation of hemicellulose, leading to relaxation of amorphous regions and weakening of intermolecular hydrogen bonding within the fiber cell wall [64,65]. Similar behavior has been reported for sedge- and grass-based fibers, where low-to-moderate thermal exposure disrupts microfibril cohesion and reduces load-bearing efficiency [66]. As the drying temperature increased to 60 - 70 °C, the tensile strength partially recovered, suggesting improved structural consolidation due to more effective moisture removal and reduced internal defects. This trend is consistent with observations in kenaf and jute fibers, where controlled drying enhances fiber packing and interfacial interactions without inducing severe structural damage [67].

At 80 °C, the significant increase in tensile strength, despite SEM evidence of micro-cracks and partial cell wall collapse, indicates the coexistence of competing mechanisms. While microstructural defects are generally associated with mechanical weakening, the overall strengthening effect can be explained by thermally induced densification and molecular reorganization within the cellulose matrix. SEM observations suggest that structural damage is localized rather than uniformly distributed, allowing intact regions of aligned cellulose microfibrils to dominate the tensile response. Concurrently, FTIR analysis supports this interpretation, showing a reduction in O–H stretching intensity (3,200 - 3,600 cm^{-1}) and a decrease in hemicellulose-associated C=O peaks (~1,730 cm^{-1}), indicating dehydration and partial removal of amorphous components. These changes promote increased relative crystallinity and improved microfibril alignment, which enhance axial load transfer efficiency [15,68]. Additionally, the persistence of lignin-related peaks (~1,240 and 1,500 - 1,600 cm^{-1}) suggests a more rigid and crosslinked matrix, further contributing to the observed increase in tensile strength [69].

This apparent contradiction between SEM-observed damage and enhanced tensile strength can therefore be reconciled by considering the balance between localized defects and bulk structural reinforcement. Similar crystallinity-driven strengthening has been reported in thermally treated lignocellulosic fibers, where increased stiffness is achieved despite partial microstructural degradation [68].

In contrast, elongation at break showed minimal variation across temperatures, with overlapping Tukey groups indicating no significant differences ($p > 0.05$).

This suggests that drying temperature primarily influences strength rather than ductility. From a practical standpoint, although 80 °C yields the highest tensile strength, the associated structural damage may compromise long-term durability. Therefore, drying at 60 - 70 °C is considered optimal, providing a balanced combination of mechanical performance and structural integrity.

Table 8 Comparative optimal drying temperatures and key fiber properties for LA fiber and selected natural fibers.

Fiber	Optimal drying temperature (°C)	Tensile strength (MPa)	Botanical family	Reference
Lepironia articulata	60	80.68 ± 11.81	Cyperaceae	This study
Jute (*Corchorus* sp.)	60 - 80	393 - 800	Malvaceae	[70]
Kenaf (*Hibiscus cannabinus*)	60 - 100	295 - 930	Malvaceae	[71]
Cyperus sp. (sedge)	~60	120 - 180	Cyperaceae	[72]
Typha sp. (cattail)	60 - 70	80 - 150	Typhaceae	[73]
Bamboo (*Bambusa* sp.)	80 - 120	140 - 800	Poaceae	[74]

The comparative analysis presented in **Table 8** demonstrates that *Lepironia articulata* (LA) fiber exhibits moderate tensile strength relative to other lignocellulosic fibers, while sharing a similar optimal drying temperature (~60 °C) with wetland fibers such as Cyperus and Typha. The tensile strength of LA (~80 MPa) falls within the lower range of Cyperaceae-type fibers but is substantially lower than that of bast fibers such as jute and kenaf, which typically exhibit tensile strengths in the range of 300 - 900 MPa. This difference can be primarily attributed to variations in cellulose content, crystallinity, and microfibril alignment, where bast fibers possess more highly ordered and aligned cellulose structures that enhance load-bearing efficiency [70,71].

In contrast, wetland fibers such as LA, Cyperus, and Typha generally exhibit a more heterogeneous cell wall structure with higher proportions of amorphous components, including hemicellulose and lignin, which contribute to lower tensile strength but improved flexibility and resilience [72,73]. The similarity in optimal drying temperatures among these fibers suggests that the critical balance between moisture removal and structural preservation occurs within a comparable thermal window (60 - 70 °C), where sufficient dehydration promotes fiber consolidation without inducing significant thermal degradation.

Although higher drying temperatures (e.g., ≥ 80 °C) can enhance tensile strength through increased cellulose crystallinity and densification, as observed in high-performance fibers such as bamboo, excessive thermal exposure may also induce microstructural defects, including cell wall collapse and micro-cracking, which can compromise long-term mechanical reliability [74]. Therefore, the mechanical performance of LA fiber should be interpreted within the context of its ecological origin and structural characteristics, positioning it as a sustainable, moderate-strength fiber suitable for semi-structural applications where flexibility and processability are advantageous over maximum strength.

FTIR spectroscopy analysis

The FTIR spectra of the LA fibers exhibited systematic changes in absorption band intensities as the drying temperature increased, reflecting alterations in chemical composition and bonding, as demonstrated in **Figure 6**.

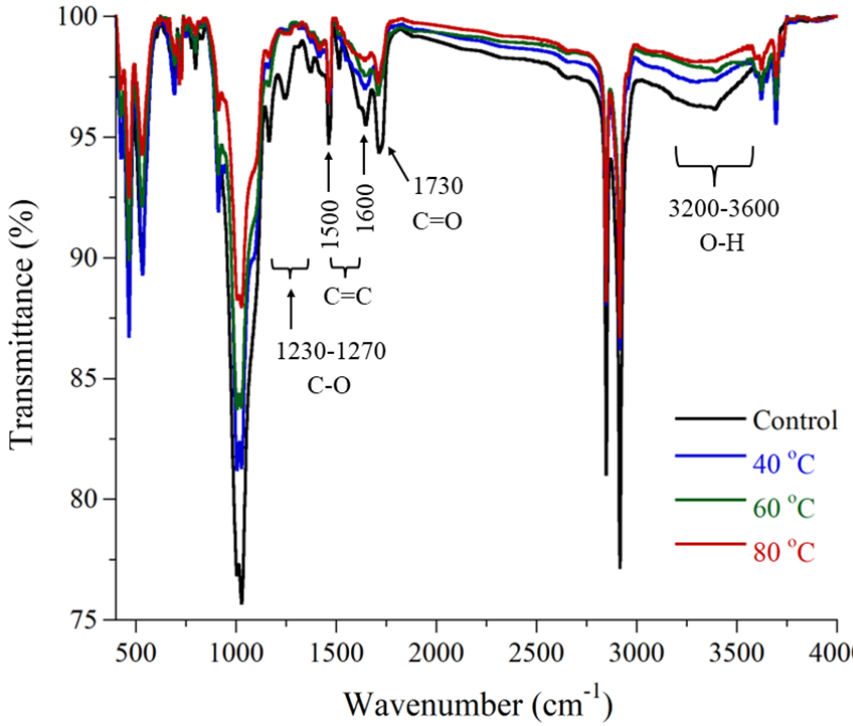

Figure 6 FTIR spectra of the LA fibers under different drying conditions (Control, 40, 60, and 80 °C).

The FTIR spectra of LA fibers exhibited systematic changes with increasing drying temperature, reflecting progressive chemical and structural transformations within the lignocellulosic matrix. The broad absorption band in the 3,200 - 3,600 cm^{-1} range, attributed to O–H stretching vibrations of adsorbed and bound water, showed a clear reduction in intensity with increasing temperature, indicating the removal of moisture and disruption of hydrogen bonding within amorphous regions [75]. Concurrently, the gradual attenuation and eventual disappearance of the carbonyl (C=O) peak around 1,730 cm^{-1} confirms the thermal degradation of hemicellulose, which is known to be more thermally labile than crystalline cellulose [76]. These changes signify a reduction in the amorphous fraction and a relative increase in cellulose ordering.

In the aromatic region (1,500 - 1,600 cm^{-1}), associated with lignin skeletal vibrations (C=C), slight shifts and intensity variations were observed, suggesting thermally induced modification of lignin structures, potentially through condensation reactions or ether linkage cleavage [77]. The persistence of the C–O stretching band in the range of 1,230 - 1,270 cm^{-1} further indicates that the lignin framework is partially preserved, although reduced intensity at higher temperatures reflects weakening intermolecular interactions within the fiber matrix [15]. Similar FTIR trends have been reported in thermally treated lignocellulosic fibers, where lignin modification is associated with increased rigidity and reduced structural flexibility [78,79].

These chemical transformations provide critical insight into the structure–property relationship observed in LA fibers. The reduction in hydroxyl groups and hemicellulose content leads to decreased moisture plasticization and enhanced intermolecular interactions within the cellulose network, promoting higher crystallinity and improved load transfer efficiency [15,72]. This mechanism explains the increase in tensile strength observed at elevated temperatures (e.g., 80 °C), despite the presence of localized structural defects identified in SEM analysis.

Importantly, the apparent contradiction between FTIR-indicated structural ordering and SEM-observed micro-cracks can be reconciled by considering scale-dependent effects. While SEM reveals localized damage such as cell wall collapse and micro-cracking, these defects are not uniformly distributed and therefore do not dominate the bulk mechanical response. Instead, the overall tensile behavior is governed by the more ordered and densified cellulose framework formed during thermal treatment. Similar phenomena have been

reported in natural fibers such as jute and kenaf, where increased crystallinity enhances stiffness and strength, even in the presence of microstructural imperfections [70,71]

Overall, FTIR analysis confirms that increasing drying temperature induces a transition from a moisture-rich, amorphous-dominated structure toward a more ordered, cellulose-rich matrix. While this transformation enhances tensile strength, excessive thermal exposure may simultaneously promote lignin condensation and structural brittleness, highlighting the importance of optimizing drying conditions to balance strength and durability.

Microstructural Analysis (SEM)

The microstructural evolution of LA fibers under different drying temperatures, as observed in SEM images (**Figure 7**), reveals a clear temperature-dependent transition in fiber morphology that is strongly correlated with FTIR-derived chemical changes. At lower drying temperatures (controlled to 40 - 50 °C), the fiber surface remains relatively smooth and structurally intact, indicating minimal disruption to the lignocellulosic matrix. This observation is consistent with FTIR results showing the persistence of hydroxyl (O–H) stretching bands (3,200 - 3,600 cm^{-1}), suggesting that bound water and hydrogen bonding networks remain largely preserved within amorphous regions [76,77].

As the drying temperature increases to 60 - 70 °C, SEM micrographs reveal gradual surface roughening, lumen shrinkage, and partial densification of the fiber structure. These morphological changes correspond closely with the reduction in O–H band intensity and attenuation of hemicellulose-associated carbonyl peaks (~1,730 cm^{-1}) observed in FTIR spectra, indicating progressive dehydration and partial degradation of amorphous components. The removal of bound water reduces internal plasticization and enhances intermolecular interactions within the cellulose framework, resulting in improved structural cohesion and load transfer efficiency. This explains the partial recovery of tensile strength observed at intermediate temperatures, where chemical stabilization and structural consolidation occur without severe damage.

At higher drying temperatures (≥ 70 °C), more pronounced microstructural degradation becomes evident. SEM images show the formation of micro-cracks, fiber pull-out, and localized cell wall collapse, which are indicative of internal stress accumulation and mechanical weakening. These features are strongly associated with FTIR-detected chemical modifications, including further reduction of hemicellulose (C=O band at ~1,730 cm^{-1}) and alterations in lignin aromatic structures (1,500 - 1,600 cm^{-1}), likely resulting from ether bond cleavage and condensation reactions under thermal exposure [15]. The persistence but reduced intensity of lignin-related C–O bands (~1,230 - 1,270 cm^{-1}) suggests that while the lignin framework remains partially intact, its bonding integrity is weakened, contributing to interfacial debonding and brittle fracture behavior.

Despite the presence of these microstructural defects, an increase in tensile strength at higher temperatures (e.g., 80 °C) can be explained by the dominance of molecular-level reorganization over localized damage. The reduction of amorphous components and moisture content promotes increased cellulose crystallinity and improved microfibril alignment, enhancing axial load-bearing capacity. SEM observations indicate that defects such as micro-cracks are not uniformly distributed, and therefore do not fully compromise the bulk mechanical response. Similar structure-property relationships have been reported in thermally treated lignocellulosic fibers such as jute, kenaf, and sedge, where increased stiffness and strength coexist with localized structural degradation [72,80,81].

In summary, the combined SEM and FTIR analyses demonstrate that drying temperature governs a critical balance between structural consolidation and degradation in LA fibers. Moderate temperatures (60 - 70 °C) promote optimal fiber integrity by enhancing molecular ordering without inducing significant damage, whereas excessive temperatures (≥ 80 °C) lead to irreversible chemical and morphological changes that may enhance strength but reduce long-term durability. These findings highlight the importance of controlled drying conditions to optimize the performance of lignocellulosic fibers for practical applications.

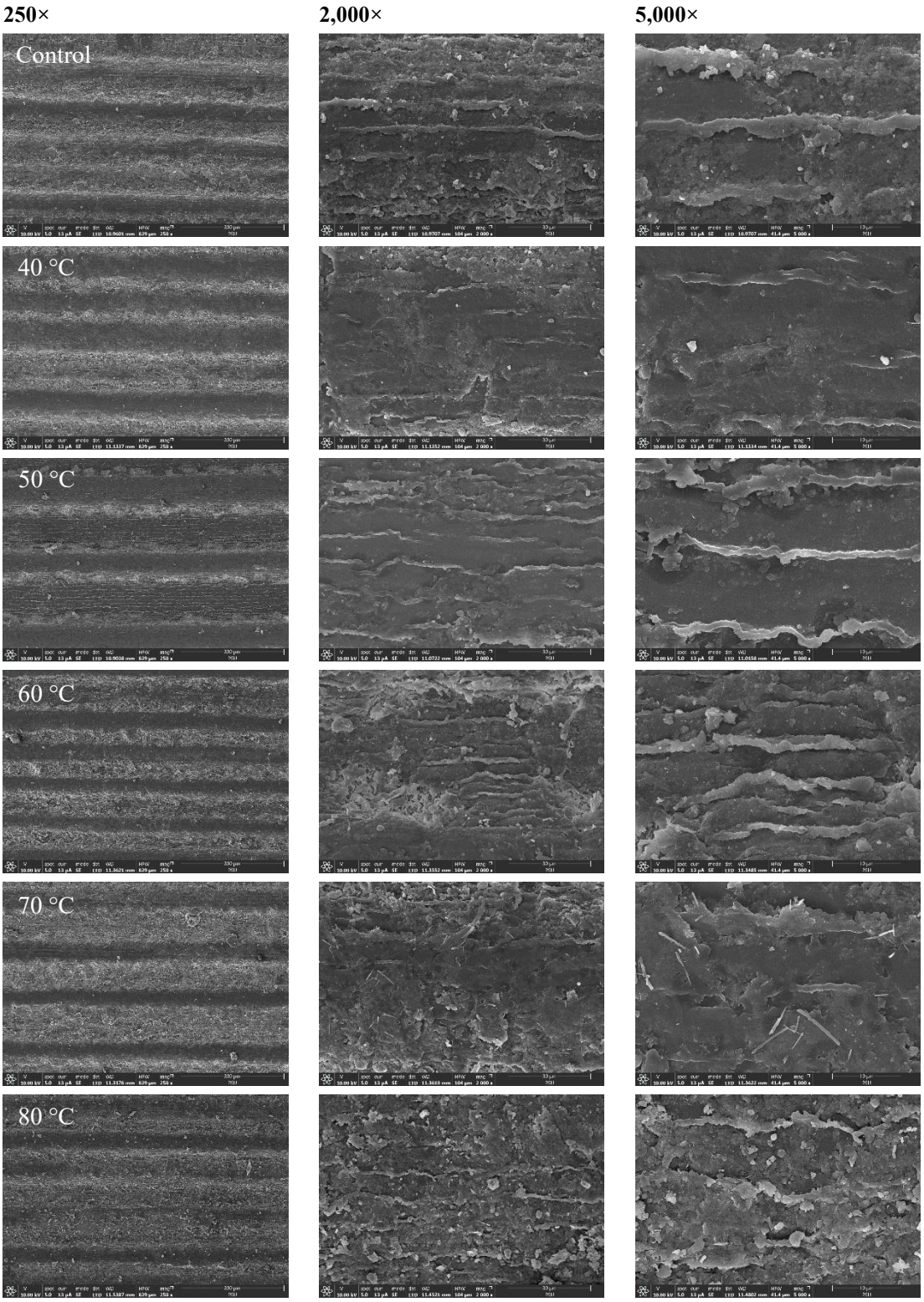

Figure 7 SEM micrographs of the LA fibers under different drying conditions (control, 40 - 80 °C).

Conclusions

This study provides a comprehensive understanding of the interrelationship between moisture sorption behavior, drying kinetics, and structural–mechanical evolution of *Lepironia articulata* fiber under controlled hot-air drying conditions. The Modified GAB model demonstrated superior predictive capability for equilibrium moisture content across a

wide range of water activities, while the Modified Page model effectively described drying kinetics governed by internal moisture diffusion. Increasing drying temperature significantly enhanced drying efficiency; however, it also induced complex physicochemical transformations within the fiber structure.

Mechanical performance exhibited a non-linear temperature dependence, reflecting the competing effects of structural degradation and molecular reorganization. At moderate temperatures (60 - 70 °C), efficient moisture removal promoted structural consolidation and maintained mechanical integrity. In contrast, higher temperatures (≥ 80 °C) induced hemicellulose degradation, lignin modification, and microstructural damage, as confirmed by FTIR and SEM analyses. Despite these defects, tensile strength increased at 80 °C due to enhanced cellulose crystallinity and microfibril alignment, indicating that bulk mechanical behavior is governed by molecular-level ordering rather than localized damage.

From a practical perspective, drying at approximately 60 °C is recommended as the optimal condition, providing a balance between drying efficiency, structural preservation, and mechanical performance. The integrated approach adopted in this study—combining sorption modeling, kinetic analysis, and multi-scale characterization—offers a robust framework for optimizing drying processes in lignocellulosic materials and supports the sustainable utilization of natural fibers in engineering and industrial applications.

Acknowledgements

This work was supported by Nakhon Si Thammarat Rajabhat University (NSTRU) and Thailand Science Research and Innovation (TSRI) through financial support from the Fundamental Fund 2567 (Grant No. NSTRU 004/2567). The authors would like to thank Nakhon Si Thammarat Rajabhat University for its instrumental role in supporting our research. We also extend our appreciation to the Division of Physics, School of Science, Walailak University, Thailand, for their instrumental support, as well as to the faculty and staff at Nakhon Si Thammarat Rajabhat University, Thailand for their continuous encouragement and resources throughout this study.

Declaration of generative AI in scientific writing

During the preparation of this work the authors used ChatGPT and QuillBot in order to check grammar. After using this tool, the authors reviewed and edited the content as needed and take full responsibility for the content of the publication

CRediT author statement

Pitchasak Chankuson: Conceptualization; Data curation; Formal analysis; Investigation; Methodology; Writing - Original draft preparation; Writing - Reviewing and Editing. **Sirikun Pethuan:** Formal analysis. **Surasak Kaew-on:** Formal analysis. **Jureeporn Yuennan:** Data curation; Formal analysis. **Chaiporn Kaew-on:** Supervision; Conceptualization; Formal analysis.

References

[1] P Domyos. 2013, *In vitro* propagation and germplasm conservation of *Lepironia articilata* (Retz.) Domin in Phru Kuan Kreng Wetlands, Nakhon Si Thammarat. Ph. D. Dissertation. Prince of Songkla University, Songkla, Thailand.

[2] AZN Elangko, J Jai, SA Ali and NM Manshor. Moisture sorption isotherm of cassava starch film incorporated with kaffir lime oil. *ASM Science Journal* 2022; **17**, 1-11.

[3] C Taveesuvun, S Tirawanichakul and Y Tirawanichakul. Equilibrium moisture content modeling and study of circulating bed drying kinetics of non-fragrant and fragrant paddy varieties. *Trends in Sciences* 2022; **19(14)**, 4950.

[4] S Simal, A Femenia, A Castell-Palou and C Rosselló. Moisture desorption isotherms of agricultural products: Influence of temperature and modeling. *Journal of Food Engineering* 2007; **79(1)**, 175-183.

[5] HA Iglesias and J Chirife. *Handbook of food isotherms: Water sorption parameters for food and food components*. Academic Press, New York, 1982.

[6] H Togrul and N Arslan. Moisture sorption isotherms and thermodynamic properties of sesame seeds. *Journal of Food Engineering* 2006; **76(3)**, 405-415.

[7] NA Aviara, OO Ajibola and KC Oni. Moisture sorption isotherms of agricultural materials: A

review. *Nigerian Food Journal* 2014; **32(1)**, 95-105.

[8] JA Olguín-Rojas, A Martinez-Candelario, ID Pérez-Landa, P Aguirre-Lara, MM González-Urrutia and M González-Pérez. Convective drying of pirul (*Schinus molle*) leaves: Kinetic modeling of water vapor and bioactive compound retention. *Processes* 2025; **13(10)**, 3259.

[9] ESG Khater, AH Bahnasawy, AE Elwakeel, AA Tantawy, A Salem, SA Marey, AM Okasha and KA Metwally. Comparative analysis of drying kinetics, thermodynamic properties, and mathematical modeling of pomegranate peel (*Punica granatum* L.) in a hybrid solar dryer and an oven dryer. *Scientific Reports* 2025; **15**, 26288.

[10] AS Muthia, DY Susanti, S Rahayoe and KQ Anyjani. Oven-drying kinetics and physical characterization of ganyong starch biofoam with various sizes of bagasse filler. *Trends in Sciences* 2025; **22(6)**, 9591.

[11] Y Joo, S Chang and S Oh. Effect of drying kinetics model on energy efficiency of drying systems. *Energy* 2024; **291**, 130390.

[12] JLC Alves, KS Prado and JMF de Paiva. Compressive and interlaminar shear strength properties of biaxial fibreglass laminates hybridized with jute fibre produced by vacuum infusion. *Journal of Natural Fibers* 2021; **18(11)**, 1772-1787.

[13] DA Asrate and AN Ali. Review on the recent trends of food dryer technologies and optimization methods of drying parameters. *Applied Food Research* 2025; **5(1)**, 100927.

[14] J Zhang, H Huo, L Zhang, Y Yang, H Li, Y Ren and Z Zhang. Effect of high-temperature hydrothermal treatment on the cellulose derived from the *Buxus* plant. *Polymers* 2022; **14(10)**, 2053.

[15] M Poletto, V Pistor, AJ Zattera and RMC Santana. Native cellulose: Structural characteristics and thermal properties. *Materials* 2014; **7(9)**, 6105-6119.

[16] IN Ramos, TRS Brandão and CLM Silva. Structural changes during air drying of fruits and vegetables. *Food Science and Technology International* 2003; **9(3)**, 201-206.

[17] X Huang, Z Zhang, Y Li, Y Yang, A Mulati, D Shataer and J Wang. The Effects of hot air and microwave drying on the structural and physicochemical properties of soluble dietary fiber from sugar beet pulp. *Foods* 2025 **14(19)**, 3435.

[18] IS Santos, BL Nascimento, RH Marino, EM Sussuchi, MP Matos and S Griza. Influence of drying heat treatments on the mechanical behavior and physico-chemical properties of mycelial biocomposite. *Composites Part B: Engineering* 2021; **217**, 108870.

[19] SM Henderson and S Pabis. Grain drying theory I temperature effects on drying coefficient. *Journal of Agricultural Engineering Research* 1961; **6**, 169-174.

[20] G Halsey. Physical adsorption on non-uniform surfaces. *Journal of Chemical Physics* 1948; **16**, 931-937.

[21] CR Oswin. The kinetic of package life. III isotherm. *Journal of Chemical Industry* 1946; **65(12)**, 419-421.

[22] DS Chung and HB Pfost. Adsorption and desorption of water vapour by cereal grains and their products. Part II: Development of the general isotherm equation. *Transactions of the ASAE* 1967; **10**, 549-557.

[23] SM Henderson. A basic concept of equilibrium moisture. *Agricultural Engineering* 1952; **33**, 29-32.

[24] RB Anderson. Modifications of the B.E.T. equation. *Journal of American Chemical Society* 1946; **68**, 686-691.

[25] JH De Boer. *The dynamical character of adsorption*. Clarendon Press, Oxford, 1953.

[26] EA Guggenheim. *Applications of statistical mechanics*. Clarendon Press, Oxford, 1966.

[27] AO Raji and JO Ojediran. Moisture sorption isotherms of two varieties of millet. *Food and Bioproducts Processing* 2011; **89(3)**, 178-184.

[28] OA Aregbesola, BS Ogunsina, AE Sofolahan and NN Chime. Mathematical modeling of thin layer drying characteristics of dika (*Irvingia gabonensis*) nuts and kernels. *Nigerian Food Journal* 2015; **33**, 83-89.

[29] GM White, IJ Ross and CG Poneleit. Fully exposed drying of popcorn. *Transactions of the ASAE* 1981; **24**, 466-0468.

[30] C Ertekin and MZ Firat. A comprehensive review of thin layer drying models used in agricultural products. *Critical Reviews in Food Science and Nutrition* 2017; **57(4)**, 701-717.

[31] EK Akpinar, Y Bicer and C Yildiz. Thin layer drying of red pepper. *Journal of Food Engineering* 2003; **59**, 99-104.

[32] İT Toğrul and D Pehlivan. Modelling of thin layer drying kinetics of some fruits under open-air sun drying process. *Journal of food Engineering* 2004; **65(3)**, 413-425.

[33] DS Chung and HB Pfost. Adsorption and desorption of water vapor by cereal grains and their products. *Transactions of the ASAE* 1967; **10**, 549-557.

[34] M Sanjeev and A Singh. Adsorption isotherms for red chili (*Capsicum annum* L.). *European Food Research and Technology*2006; **223**, 849-852.

[35] K Strømdahl. 2000, Water sorption in wood and plant fibres. Ph. D. Dissertation. Technical University of Denmark, Lyngby, Denmark.

[36] GY Farag, EMA Abou Taleb and T Hamouda. Natural fibers extraction methods and properties: A review. *Egyptian Journal of Chemistry* 2025; **68(3)**, 445-464.

[37] MJ Mohd Nor and A Putra. *Lepironia articulata* as a sustainable acoustic absorber. *Research Progress in Mechanical and Manufacturing Engineering* 2022; **2(2)**, 201-212.

[38] MS Alamri, AA Mohamed, S Hussain, MA Ibraheem and AA Abdo Qasem. Determination of moisture sorption isotherm of crosslinked millet flour and oxirane using GAB and BET. *Journal of Chemistry* 2018; **2018(1)**, 2369762.

[39] M Chanpet, N Rakmak, N Matan and C Siripatana. Effect of air velocity, temperature, and relative humidity on drying kinetics of rubberwood. *Heliyon* 2020; **6(10)**, e05151.

[40] W Zhao, J Zhang, W Zhang, J Wang and G Wang. Changes in the structural composition and moisture-adsorption properties of mechanically rolled bamboo fibers. *Materials* 2022; **15(10)**, 3463.

[41] Y Hfaiedh, H Hachem and D Mihoubi. Drying kinetics and sorption isotherms of biocomposite materials: Experimental investigation and modeling analysis. *ACS Omega* 2024; **9(42)**, 42957-42969.

[42] T Defraeye. Advanced computational modeling of drying processes - a review. *Applied Energy* 2014; **131**, 323-344.

[43] Y Dadmohammadi and AK Datta. Food as porous media: A review of the dynamics of porous properties during processing. *Food Reviews International* 2022; **38(5)**, 953-985.

[44] IP Owoh, WI Okonkwo, CN Anyanwu, O Ojike and NI Nwagugu. A review on modeling the drying kinetics of agricultural bio materials and wastes. *International Journal of Research and Innovation in Applied Science* 2025; **10(5)**, 954-966.

[45] CM de Alcântara, IdS Moreira, MT Cavalcanti, RP Lima, HV Moura, R da Silva Neves, CAL Cassimiro, JJA Martins, FR da Costa Batista and EM Pereira. Mathematical modeling of drying kinetics and technological and chemical properties of *Pereskia* sp. leaf powders. *Processes* 2024; **12**, 2077.

[46] X Zhang, Y Liu and Q Li. Research on the prediction model and formation law of drying cracks of paddy based on multi-physical field coupling. *Agriculture* 2025; **15(4)**, 383.

[47] Y Buelvas Arrieta, L Díaz Reyes, C Ávila-Díaz, J Altamiranda Suárez, O Rivero-Romero and J Unfried-Silgado. Effects of drying temperature, mercerizing, and coating on the properties of Colombian Coir fibers and their interfacial adhesion with polylactic acid. *Scientific Reports* 2025; **15**, 32346.

[48] K Prawiranto, T Defraeye, D Derome, A Bühlmann, S Hartmann, P Verboven, B Nicolai and J Carmeliet. Impact of drying methods on the changes of fruit microstructure unveiled by X-ray micro-computed tomography. *RSC Advances* 2019; **9(19)**, 10606-10624.

[49] I Doymaz. Evaluation of some thin-layer drying models of persimmon slices (*Diospyros kaki* L.). *Energy Conversion and Management* 2012; **56**, 199-205.

[50] Z Erbay and F Icier. A review of thin layer drying of foods: theory, modeling, and experimental results. *Critical Reviews in Food Science and Nutrition* 2010; **50(5)**, 441-464.

[51] AS Mujumdar. *Handbook of industrial drying.* 4th ed. CRC Press, Boca Raton, United States, 2014.

[52] Z Wang, J Sun, F Chen, X Liao, G Zhao, J Wu and X Hu. Mathematical modeling on thin layer drying of apple pomace. *Food Research International* 2007; **40**, 39-46.

[53] AO Abioye, AA Adekunle, OA Jeremiah, IO Bazambo, OB Adetoro, KO Mustapha, CF Onyeka and TA Ayorinde. Modelling the influence of temperature on the drying kinetics of Turmeric slices. *Croatian Journal of Food Science and Technology* 2021; **13(2)**, 167-175.

[54] M Nowacka, M Dadan and U Tylewicz. Drying Technologies in Food Processing. *Applied Sciences* 2023; **13(19)**, 10597.

[55] S Nansereko, J Muyonga and YB Byaruhanga. Influence of drying methods on jackfruit drying behavior and dried products physical characteristics. *International Journal of Food Science* 2022; **2022(1)**, 8432478.

[56] K Prasad and P Ankita. Temperature dependent dehydration kinetics and effective diffusivity of Spinach leaves. *Indian Journal of Biotechnology* 2017; **13(4)**, 142.

[57] W Senadeera, J Banks, G Adiletta and K Brewer. Microstructural approach application for morphological change determinations of grapes during drying. *Processes* 2024; **12(4)**, 720.

[58] K Limpaiboon. Mathematical modeling of drying kinetics of bird's eye chilies in a convective hot-air dryer. *Walailak Journal of Science and Technology* 2020; **12(2)**, 219.

[59] OO George, KR Erick, OA Patrick and BG Benson. Evaluation of thin layer models for simulating drying kinetics of black nightshade seeds in a solar-exhaust gas greenhouse dryer. *Bioprocess Engineering* 2023, **7(1)**, 10-31.

[60] M Kaveh and P Abbaszadeh. Review of mathematical modelling of thin layer drying processes. *International Journal of Current Engineering and Scientific Research* 2015; **2(11)**, 96-107.

[61] K Górnicki, A Kaleta and A Choińska. Suitable model for thin-layer drying of root vegetables and onion. *International Agrophysics* 2020, **34(1)**, 79-86.

[62] M Krokida and Z Maroulis. Quality changes during drying of food materials. *Drying Technology in Agriculture and Food Sciences* 2000; **4(2)**, 61-68.

[63] FRB Martinelli, MG Pariz, R de Andrade, SR Ferreira, FA Marques, SN Monteiro and ARG de Azevedo. Influence of drying temperature on coconut-fibers. *Scientific Reports* 2024; **14**, 6421.

[64] O Faruk, AK Bledzki, HP Fink and M Sain. Biocomposites reinforced with natural fibers: 2000 - 2010. *Progress in Polymer Science* 2012; **37(11)**, 1552-1596.

[65] D Ray, BK Sarkar, AK Rana and NR Bose. Effect of alkali treated jute fibres on composite properties. *Bulletin of Materials Science* 2001; **24(2)**, 129-135.

[66] KL Pickering, MGA Efendy and TM Le. A review of recent developments in natural fibre composites and their mechanical performance. *Composites Part A: Applied Science and Manufacturing* 2016; **83**, 98-112.

[67] M Thiruchitrambalam, A Alavudeen, A Athijayamani, N Venkateshwaran and AE Perumal. Improving mechanical properties of banana/kenaf hybrid fiber reinforced composites using sodium hydroxide treatment. *Materials & Design* 2012; **47**, 283-290.

[68] H Yang, R Yan, H Chen, DH Lee and C Zheng. Characteristics of hemicellulose, cellulose and lignin pyrolysis. *Fuel* 2007; **86(12-13)**, 1781-1788.

[69] D Kocaefe, S Poncsak and Y Boluk. Effect of thermal treatment on the chemical composition and mechanical properties of birch and aspen. *BioResources* 2008; **3(2)**, 517-537.

[70] DU Shah. Developing plant fibre composites for structural applications by optimising composite parameters: a critical review. *Journal of Materials Science* 2013; **48(18)**, 6083-6107.

[71] HM Akil, MF Omar, AM Mazuki, SZ Safiee, ZM Ishak and AA Bakar. Kenaf fiber reinforced composites: A review. *Materials & Design* 2011; **32(8-9)**, 4107-4121.

[72] N Reddy and Y Yang. Biofibers from agricultural byproducts for industrial applications. *Trends in Biotechnology* 2005; **23(1)**, 22-27.

[73] HPS Abdul Khalil, IUH Bhat, M Jawaid, A Zaidon, D Hermawan and YS Hadi. Bamboo fibre reinforced biocomposites: A review. *Materials & Design* 2012; **42**, 353-368.

[74] Y Yu, B Fei, B Zhang and X Yu. Cell-wall mechanical properties of bamboo investigated by nanoindentation. *Wood Science and Technology* 2007; **39(4)**, 527-535.

[75] W Dawmanee, S Ruang-on and P Nuengmatcha. Preparation and characterization of activated carbon from *Lepironia articulata* (Retz.) Domin waste as an adsorbent for methylene blue dye removal from wastewater. *Asian Journal of Chemistry* 2024; **36(2)**, 294-300.

[76] A Şencan and M Kılıç. Investigation of the changes in surface area and FT-IR spectra of activated carbons obtained from hazelnut shells by physicochemical treatment methods. *Journal of Chemistry* 2015; **2015**, 651651.

[77] J Montoya Berrio, J Negrete Martínez, J Altamiranda Suárez, C Ávila Díaz, O Rivero-Romero and J Unfried-Silgado. Influence of drying temperature on the properties of Colombian banana pseudostem fibers for its potential use as reinforcement in composite materials. *Scientific Reports* 2024; **14**, 25180.

[78] A Célino, S Fréour, F Jacquemin and P Casari. The hygroscopic behavior of plant fibers: A review. *Frontiers in Chemistry* 2014; **1**, 43.

[79] A Bakkour, SE Ouldoukhitine, P Biwole and S Amziane. A review of multi-scale hygrothermal characteristics of plant-based building materials. *Construction and Building Materials* 2024; **412**, 134850.

[80] MM Kabir, H Wang, KT Lau and F Cardona. Chemical treatments on plant-based natural fibre reinforced polymer composites: An overview. *Composites Part B: Engineering* 2012; **43(7)**, 2883-2892.

[81] M Poletto, AJ Zattera, MMC Forte and RMC Santana. Thermal decomposition of wood: Influence of wood components and cellulose crystallite size. *Bioresource Technology* 2014; **109**, 148-153.